NASA Technical Paper 3362

CECOM Technical Report 93-E-2

August 1993

Analysis of Microstrip Patch Antennas With Nonzero Surface Resistance

David G. Shively
and M. C. Bailey

NASA Technical Paper 3362

CECOM Technical Report 93-E-2

1993

Analysis of Microstrip Patch Antennas With Nonzero Surface Resistance

David G. Shively
Joint Research Program Office
Electronics Integration Directorate
Communications Electronics Command
Langley Research Center
Hampton, Virginia

M. C. Bailey
Langley Research Center
Hampton, Virginia

Abstract

The scattering properties of a microstrip patch antenna with nonzero surface impedance are examined. The electric field integral equation for a current element on a grounded dielectric slab is developed for a rectangular geometry by using Galerkin's technique with subdomain piecewise linear basis functions. The integral equation includes a resistive boundary condition on the surface of the patch. The incident field on the patch is expressed as a function of incidence angle. The resulting system of equations is then solved for the unknown current modes on the patch, and the radar cross section is calculated for a given scattering angle. Theoretical results in the form of radar cross section as a function of frequency are compared with results measured at the NASA Langley Research Center.

Symbols

d	thickness of dielectric slab
$\vec{E}_{\tan}^{\text{inc}}$	tangential components of incident electric field
$\vec{E}_{\tan}^{\text{scat}}$	tangential components of scattered electric field
E_{θ}^{mn}	$\widehat{\theta}$ component of electric field
E_{ϕ}^{mn}	$\widehat{\phi}$ component of electric field
F^{mn}	Fourier transform of current mode mn
$\overleftrightarrow{G}$	dyadic Green's function
I^{mn}	amplitude of mode mn
$\vec{J}$	surface current on microstrip patch antenna
j	$= \sqrt{-1}$
K, α	variables of integration in cylindrical coordinates
K_o	propagation constant for free space, $2\pi/\lambda_o$
K_x	spectral domain transformation variable for x-direction
K_y	spectral domain transformation variable for y-direction
K_1	propagation constant for dielectric slab in z-direction
K_2	propagation constant for free space in z-direction
L_x	dimension of the patch in x-direction
L_y	dimension of the patch in y-direction
M	number of subdivisions in x-direction
mn, pq	indices specifying the subdomain basis functions on patch
N	number of subdivisions in y-direction
R	resistance matrix representing surface resistance on patch
R_s	surface resistance on microstrip patch antenna
T_e	characteristic equation for transverse electric modes
T_m	characteristic equation for transverse magnetic modes
V^{mn}	component of excitation voltage vector
(x, y, z)	coordinates of field point
(x', y', z')	coordinates of source point
$\widehat{x}$	unit vector in x-direction
x_m, y_n	coordinates of current mode mn
Δx	cell size in x-direction
$\widehat{y}$	unit vector in y-direction
Δy	cell size in y-direction
Z	impedance matrix to be solved
Z_o	impedance of free space, 377 Ω

$\widehat{z}$	unit vector in z-direction
ϵ_r	relative permittivity of dielectric slab
θ^i, ϕ^i	incident angle of electromagnetic wave
Λ	piecewise linear function for current on patch
λ_o	wavelength of electromagnetic field in free space
μ_o	permeability of free space
Π	pulse function for the current on patch
$\sigma_{\theta\theta}$	$\widehat{\theta}$-polarized backscatter from $\widehat{\theta}$-polarized incident field
$\sigma_{\theta\phi}$	$\widehat{\phi}$-polarized backscatter from $\widehat{\theta}$-polarized incident field
$\sigma_{\phi\theta}$	$\widehat{\theta}$-polarized backscatter from $\widehat{\phi}$-polarized incident field
$\sigma_{\phi\phi}$	$\widehat{\phi}$-polarized backscatter from $\widehat{\phi}$-polarized incident field
ω	radian frequency of electromagnetic field

Introduction

Spectral domain Green's functions, which describe the electric field radiated by a current source on a grounded dielectric slab, were introduced in the early 1980's. This allowed the development of a moment method for analyzing perfectly conducting microstrip patch antennas. This technique accurately accounts for dielectric thickness, dielectric losses, and surface wave losses and can be extended to include the effects of a cover layer of a different dielectric constant on top of the antenna. Because of the spectral nature of the technique, it can easily be extended to model an infinite array of patches by examining only a single unit cell. Also of interest are the effects of lossy materials on the antenna. Lossy materials on the antenna will decrease the efficiency of the antenna, and hence the gain of the antenna will be lowered. This decrease in gain also means that the scattering from the antenna will be decreased. As losses are added to an antenna, other properties of the antenna, such as bandwidth, input impedance, and radiation patterns, will also be altered.

The moment method technique incorporates either subdomain or entire domain expansion functions in order to model the current on the patch. Bailey and Deshpande (refs. 1–3) have used subdomain expansion functions in order to model rectangular patches. Many other authors (refs. 4–13) have used entire domain expansion functions in order to model rectangular and circular patches. Bailey and Deshpande (ref. 14) have also used entire domain expansion functions to model an elliptical patch. The majority of this work has examined the input impedance and scattering properties of perfectly conducting patches both as single radiators and as infinite arrays. Hansen and Janhsen (ref. 15) have included a space-varying surface impedance when modeling a microstrip feed network.

A technique similar to the spectral domain method uses spatial domain Green's functions with subdomain expansion functions in order to model microstrip structures. The disadvantage of this technique is that it is not easily extended to examine infinite arrays. A number of authors (refs. 16–19) have used this technique to model microstrip patch antennas as single radiators. Mosig (ref. 18) has mentioned that conductor losses can be included in this model, but no results have been presented.

The boundary condition for the electric field on a thin resistive sheet has been examined by Senior (refs. 20–23) and is valid as long as the sheet is electrically thin. Using this type of boundary condition, several authors (refs. 24–27) have examined the scattering response of resistive strips and tapered resistive strips. This approach has also been used in order to study frequency selective surfaces (refs. 28–30). The same model for the surface resistance has been used in the study of superconducting materials and strip lines (refs. 31 and 32).

This paper will describe spectral domain analysis of imperfectly conducting microstrip patch antennas by using subdomain basis functions to model the patch current density. To simplify the analysis, the antenna feed will not be considered. The antenna is considered to be open circuited from the feed network, i.e., the feed impedance is infinite. Results are presented in the form of radar cross section as a function of frequency for a few representative cases and are compared with measured results.

Theory

The geometry of a rectangular microstrip patch antenna is shown in figure 1. The patch is assumed to be electrically thin and located on a grounded dielectric slab of infinite extent. The dielectric slab has relative permittivity ϵ_r, relative permeability μ_r,

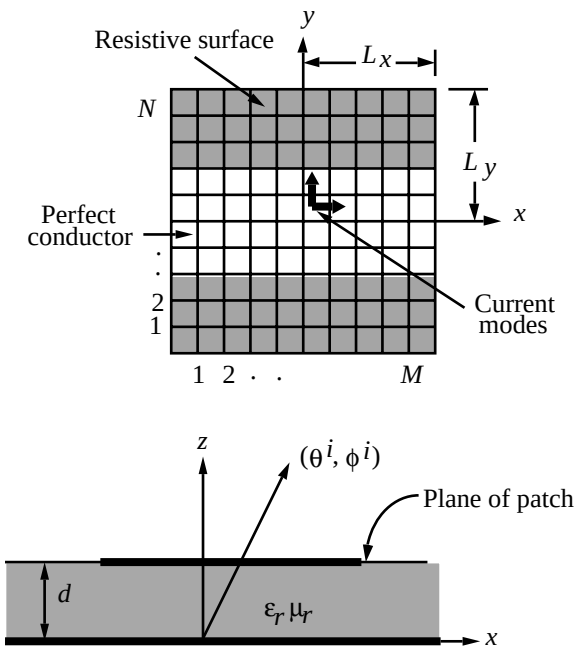

Figure 1. Geometry of a microstrip antenna with arbitrary surface resistance.

and thickness d. The standard $e^{j\omega t}$ time convention is assumed. The boundary condition on the patch is given by (ref. 23)

$$\vec{E}_{\tan}^{\text{inc}} + \vec{E}_{\tan}^{\text{scat}} = R_s \vec{J} \tag{1}$$

The incident field is the field at the patch location due to an incident plane wave. The right side of equation (1) represents the field dissipated on the patch. The surface resistance R_s is, in general, a function of x and y and is equal to zero for a perfectly conducting patch. The scattered field is the field radiated by the electric current on the patch. Following a notation similar to that of Aberle and Pozar (ref. 9), the scattered field is found from the currents excited on the patch as

$$\vec{E}^{\text{scat}}(x,y,z) = \iiint_{V'} \overleftrightarrow{G}\left(x,y,z|x',y',z'\right) \cdot \vec{J}\left(x',y',z'\right)\, dx', dy', dz' \tag{2}$$

where $\overleftrightarrow{G}$ is the dyadic Green's function for a current element on a grounded dielectric slab and $\vec{J}$ is the unknown vector electric current density on the patch. The dyadic Green's function can be written in the form

$$\begin{aligned}\overleftrightarrow{G} = {} & \hat{x}G_{xx}\hat{x} + \hat{x}G_{xy}\hat{y} + \hat{x}G_{xz}\hat{z} + \hat{y}G_{yx}\hat{x} \\ & + \hat{y}G_{yy}\hat{y} + \hat{y}G_{yz}\hat{z} + \hat{z}G_{zx}\hat{x} + \hat{z}G_{zy}\hat{y} + \hat{z}G_{zz}\hat{z}\end{aligned} \tag{3}$$

where

$$G_{ab} = \frac{1}{4\pi^2}\int_{-\infty}^{\infty}\int_{-\infty}^{\infty} \widetilde{G}_{ab}\left(K_x, K_y, z|z'\right) \times e^{jK_x(x-x')} e^{jK_y(y-y')}\, dK_x\, dK_y \tag{4}$$

and a and b can be x, y, or z.

The components of the Green's function are given by

$$\widetilde{G}_{xx}\left(K_x, K_y, d|d\right) = \frac{-jZ_o}{K_o}\frac{K_1K_2K_x^2T_e + K_o^2K_y^2T_m}{\beta^2 T_m T_e}\sin\left(K_1 d\right) \tag{5}$$

$$\widetilde{G}_{xy}\left(K_x, K_y, d|d\right) = \frac{jZ_o}{K_o}\frac{K_xK_y\left(K_o^2T_m - K_1K_2T_e\right)}{\beta^2 T_m T_e}\sin\left(K_1 d\right) \tag{6}$$

$$\widetilde{G}_{yx}\left(K_x, K_y, d|d\right) = \widetilde{G}_{xy}\left(K_x, K_y, d|d\right) \tag{7}$$

$$\widetilde{G}_{yy}\left(K_x, K_y, d|d\right) = \frac{-jZ_o}{K_o}\frac{K_1K_2K_y^2T_e + K_o^2K_x^2T_m}{\beta^2 T_m T_e}\sin\left(K_1 d\right) \tag{8}$$

$$\widetilde{G}_{zx}\left(K_x, K_y, d|d\right) = \frac{-jZ_o}{K_o}\frac{K_xK_1}{T_m}\sin\left(K_1 d\right) \tag{9}$$

$$\widetilde{G}_{zy}\left(K_x, K_y, d|d\right) = \frac{-jZ_o}{K_o}\frac{K_yK_1}{T_m}\sin\left(K_1 d\right) \tag{10}$$

where

$$T_m = \epsilon_r K_2 \cos\left(K_1 d\right) + jK_1 \sin\left(K_1 d\right) \tag{11}$$

$$T_e = K_1 \cos\left(K_1 d\right) + jK_2 \sin\left(K_1 d\right) \tag{12}$$

$$K_1 = \sqrt{\epsilon_r K_o^2 - \beta^2} \qquad \left(\text{Im}\left(K_1\right) \le 0\right) \tag{13}$$

$$K_2 = \sqrt{K_o^2 - \beta^2} \qquad \left(\text{Im}\left(K_2\right) \le 0\right) \tag{14}$$

$$\beta = \sqrt{K_x^2 + K_y^2} \tag{15}$$

The remaining terms of the Green's function are not needed in the present analysis. Details of the derivation of the Green's function can be found in reference 3. Additional forms of the Green's function

are available in the literature and include such things as a dielectric covering above the antenna (ref. 10) and a uniaxial substrate (ref. 13).

The current density $\vec{J}$ is modeled as a summation of piecewise linear subdomain basis functions known as rooftop basis functions. This approach is in contrast to using entire domain basis functions that span the entire patch. Entire domain basis functions, such as sines and cosines, are useful for analyzing rectangular or circular patches but become cumbersome when used for other shapes. Mathematically, the subdomain basis functions for the components of the current density are described as

$$J_x = \sum_{m=1}^{M}\sum_{n=1}^{N+1} J_x^{mn} = \sum_{m=1}^{M}\sum_{n=1}^{N+1} I_x^{mn}\Lambda^m(x)\,\Pi^n(y) \tag{16}$$

$$J_y = \sum_{m=1}^{M+1}\sum_{n=1}^{N} J_y^{mn} = \sum_{m=1}^{M+1}\sum_{n=1}^{N} I_y^{mn}\Lambda^n(y)\,\Pi^m(x) \tag{17}$$

where the functions Λ and Π are "triangle" and "pulse" functions, respectively, and are expressed as

$$\Lambda^m(x) = \begin{cases} 1+(x-x_m)/\Delta x & (x_m-\Delta x \le x \le x_m) \\ 1-(x-x_m)/\Delta x & (x_m \le x \le x_m+\Delta x) \\ 0 & \text{(Otherwise)} \end{cases} \tag{18}$$

$$\Pi^n(y) = \begin{cases} 1 & (y_n-\Delta y \le y \le y_n) \\ 0 & \text{(Otherwise)} \end{cases} \tag{19}$$

where $\Delta x = 2L_x/(M+1)$ and $\Delta y = 2L_y/(N+1)$. Each single subdomain on the patch is specified by a pair of indices mn that also correspond to the coordinates x_m and y_n.

After equations (2) and (4) are combined, the order of integration may be changed and the basis functions that represent the patch current density may be transformed into the K_x, K_y domain. These spectral domain current density functions are given by

$$\widetilde{J}_x(K_x,K_y) = \sum_{m=1}^{M}\sum_{n=1}^{N+1} I_x^{mn} F_x^{mn}(K_x,K_y) \tag{20}$$

$$\widetilde{J}_y(K_x,K_y) = \sum_{m=1}^{M+1}\sum_{n=1}^{N} I_y^{mn} F_y^{mn}(K_x,K_y) \tag{21}$$

where

$$F_x^{mn}(K_x,K_y) = \Delta x\ \Delta y \left[\frac{\sin(K_y\Delta y/2)}{K_y\Delta y/2}\right]\left[\frac{\sin(K_x\Delta x/2)}{K_x\Delta x/2}\right]^2 \times \exp[-jK_x x_m - jK_y y_n + jK_y(\Delta y/2)] \tag{22}$$

$$F_y^{mn}(K_x,K_y) = \Delta x\ \Delta y \left[\frac{\sin(K_y\Delta y/2)}{K_y\Delta y/2}\right]^2\left[\frac{\sin(K_x\Delta x/2)}{K_x\Delta x/2}\right] \times \exp[-jK_x x_m - jK_y y_n + jK_y(\Delta x/2)] \tag{23}$$

By using Galerkin's method, the resulting equations are then "tested" with the same set of basis functions, $\vec{J}^{pq} = J_x^{pq}\hat{x} + J_y^{pq}\hat{y}$, yielding a set of simultaneous equations that can be solved by standard techniques. The boundary condition equation (1), becomes

$$\iint_S \vec{J}^{pq}\cdot\vec{E}_{\tan}^{\text{inc}}\,dx\,dy = -\iint_S \vec{J}^{pq}\cdot\vec{E}_{\tan}^{\text{scat}}\,dx\,dy + \iint_S \vec{J}^{pq}\cdot R_s\vec{J}^{mn}\,dx\,dy \tag{24}$$

and as p and q are varied over each subdomain, the resulting system of equations can be shown in matrix notation as

$$\begin{bmatrix}[V_x^{pq}]\\ [V_y^{pq}]\end{bmatrix} = \begin{bmatrix}[Z_{xx}^{pqmn}] & [Z_{xy}^{pqmn}]\\ [Z_{yx}^{pqmn}] & [Z_{yy}^{pqmn}]\end{bmatrix}\begin{bmatrix}[I_x^{mn}]\\ [I_y^{mn}]\end{bmatrix} + \begin{bmatrix}[R_{xx}^{pqmn}] & 0\\ 0 & [R_{yy}^{pqmn}]\end{bmatrix}\begin{bmatrix}[I_x^{mn}]\\ [I_y^{mn}]\end{bmatrix} \tag{25}$$

The impedance matrix terms are given by

$$Z_{xx}^{pqmn} = \frac{-1}{4\pi^2}\int_{-\infty}^{\infty}\int_{-\infty}^{\infty}\widetilde{G}_{xx}(K_x,K_y,d|d)\,F_x^{mn}(K_x,K_y) \times F_x^{pq}(-K_x,-K_y)\,dK_x dK_y \tag{26}$$

$$Z_{xy}^{pqmn} = \frac{-1}{4\pi^2}\int_{-\infty}^{\infty}\int_{-\infty}^{\infty}\widetilde{G}_{xy}(K_x,K_y,d|d)\,F_y^{mn}(K_x,K_y) \times F_x^{pq}(-K_x,-K_y)\,dK_x dK_y \tag{27}$$

$$Z_{yx}^{pqmn} = \frac{-1}{4\pi^2}\int_{-\infty}^{\infty}\int_{-\infty}^{\infty}\widetilde{G}_{yx}(K_x,K_y,d|d)\,F_x^{mn}(K_x,K_y) \times F_y^{pq}(-K_x,-K_y)\,dK_x dK_y \tag{28}$$

$$Z_{yy}^{pqmn} = \frac{-1}{4\pi^2}\int_{-\infty}^{\infty}\int_{-\infty}^{\infty}\widetilde{G}_{yy}\left(K_x,K_y,d|d\right)F_y^{mn}\left(K_x,K_y\right) \times F_y^{pq}\left(-K_x,-K_y\right)\,dK_x dK_y \tag{29}$$

The integrations in equations (26)–(29) must be done numerically but can be simplified with the following change of variables

$$\left.\begin{aligned} K_x &= K\cos\alpha \\ K_y &= K\sin\alpha \end{aligned}\right\} \tag{30}$$

With this change of variables, the integrals are changed to the form

$$\int_{-\infty}^{\infty}\int_{-\infty}^{\infty}[\quad]\,dK_x\,dK_y = \int_0^{2\pi}\int_0^{\infty}[\quad]K\,dK\,d\alpha \tag{31}$$

The integration from 0 to 2π may be further reduced to an integration from 0 to $\pi/2$ by using the even and odd properties of the integrand. It should be noted that each of the four submatrices of the impedance matrix are of a modified block Toeplitz form. This means that only the first row of each submatrix must be calculated by numerical integration. The remaining terms of each submatrix can be filled with the first row terms, thus reducing the time needed to calculate the impedance matrix. Furthermore, it can be shown that $Z_{xy}^{pqmn} = Z_{yx}^{mnpq}$, which further reduces the computer time.

The terms of the resistance matrix are given by

$$R_{xx}^{pqmn} = \int_{x_p-\Delta x}^{x_p+\Delta x}\int_{y_q-\Delta y}^{y_q} R_s\left(x,y\right)\Lambda^p\left(x\right) \times \Pi^q\left(y\right)\Lambda^m\left(x\right)\Pi^n\left(y\right)\,dy\,dx \tag{32}$$

$$R_{yy}^{pqmn} = \int_{x_p-\Delta x}^{x_p}\int_{y_q-\Delta y}^{y_q+\Delta y} R_s\left(x,y\right)\Pi^p\left(x\right) \times\left(x\right)\Lambda^q\left(y\right)\Pi^m\left(x\right)\Lambda^n\left(y\right)\,dy\,dx \tag{33}$$

Note that the R_{xx}^{pqmn} terms will equal zero if $p > (m+1)$, $p < (m-1)$, or $q \neq n$. Likewise, the R_{yy}^{pqmn} terms will equal zero if $q > (n+1)$, $q < (n-1)$, or $p \neq m$. If R_s is constant in the pq subdomain, equation (32) reduces to

$$R_{xx}^{pqmn} = \begin{cases} \frac{R_s\,\Delta x\,\Delta y}{6} & (p=m+1, p=m-1, q=n) \\ \frac{2R_s\,\Delta x\,\Delta y}{3} & (p=m, q=n) \\ 0 & \text{(Otherwise)} \end{cases} \tag{34}$$

and equation (33) reduces to

$$R_{yy}^{pqmn} = \begin{cases} \frac{R_s\,\Delta x\,\Delta y}{6} & (q=n+1, q=n-1, p=m) \\ \frac{2R_s\,\Delta x\,\Delta y}{3} & (q=n, p=m) \\ 0 & \text{(Otherwise)} \end{cases} \tag{35}$$

If the surface resistance R_s varies across the patch as a function of x and y, the integrals may be evaluated by numerical integration. It is important to note that the terms of the resistance matrix do not depend on frequency.

In order to examine the scattering from a microstrip patch antenna it is necessary to evaluate the left side of equation (25). Each member of the excitation vector can be written as

$$V^{pq} = \iint_S \vec{J}^{pq}\cdot\vec{E}^{\text{inc}}\,dx\,dy \tag{36}$$

By reciprocity, this can be rewritten as (ref. 13)

$$V^{pq} = \frac{-4\pi\vec{E}^{pq}\cdot\vec{E}_o}{j\omega\mu_o} \tag{37}$$

where $\vec{E}_o$ is the vector amplitude of the incident plane wave, $\vec{E}^{pq}$ is the far-field radiation from vector current mode pq on the patch, and $-4\pi/j\omega\mu_o$ is the required strength of an infinitesimal dipole source to produce a unit amplitude plane wave. The factor $e^{-jK_o r}/r$ has been suppressed in equation (37). The incident plane wave is assumed to have unit amplitude and is from the direction (θ^i,ϕ^i) in spherical coordinates with components E_θ and E_ϕ.

The fields radiated by a current mode on the patch can be found with the Green's function defined above. The field at the point (x,y,z) from an impulse current source located at the point (x',y',d) is given by

$$E_a\left(x,y,z\right) = \frac{1}{4\pi^2}\int_{-\infty}^{\infty}\int_{-\infty}^{\infty}\widetilde{G}_{ab}e^{jK_x(x-x')} \times e^{jK_y(y-y')}e^{-jK_z(z-d)}\,dK_x dK_y \tag{38}$$

where a can be either x, y, or z and b is x or y. These integrals can be evaluated by the method of stationary phase and then integrated over the extent of each basis function to give the fields radiated by that basis function in the presence of the grounded dielectric slab (ref. 13). Once this has been done and the resulting equations converted to spherical

coordinates, the far-field components due to a single $\hat{x}$-directed current mode, mode mn, are

$$E_\theta^{mn}(r,\theta,\phi) = \frac{Z_o}{2\pi}\left[\frac{e^{-jK_o r}}{r}\right] e^{jK_2 d\cos\theta} \times \frac{K_1 K_o \cos\phi \sin(K_1 d)}{T_m} F_x^{mn}(K_x, K_y) \quad (39)$$

$$E_\phi^{mn}(r,\theta,\phi) = \frac{Z_o}{2\pi}\left[\frac{e^{-jK_o r}}{r}\right] e^{jK_2 d\cos\theta} \times \frac{-K_o^2 \sin\phi \sin(K_1 d)}{T_e} F_x^{mn}(K_x, K_y) \quad (40)$$

where K_x and K_y are evaluated at the stationary phase points:

$$\left.\begin{aligned} K_x &= -K_o \sin\theta\cos\phi \\ K_y &= -K_o \sin\theta\sin\phi \end{aligned}\right\} \quad (41)$$

Similarly, the fields radiated by a single $\hat{y}$-directed current mode, mode mn, are given by

$$E_\theta^{mn}(r,\theta,\phi) = \frac{Z_o}{2\pi}\left[\frac{e^{-jK_o r}}{r}\right] e^{jK_2 d\cos\theta} \times \frac{K_1 K_o \sin\phi \sin(K_1 d)}{T_m} F_y^{mn}(K_x, K_y) \quad (42)$$

$$E_\phi^{mn}(r,\theta,\phi) = \frac{Z_o}{2\pi}\left[\frac{e^{-jK_o r}}{r}\right] e^{jK_2 d\cos\theta} \times \frac{K_o^2 \cos\phi \sin(K_1 d)}{T_e} F_y^{mn}(K_x, K_y) \quad (43)$$

where K_x and K_y are the same as in equation (39). By using equations (39)–(43) in equation (37), the left-hand side of equation (25) can be determined.

Once the impedance matrix and the resistance matrix have been calculated, the results are added together to form a system of simultaneous equations. The excitation vector is then evaluated for the given incidence angle, and the system is solved for the unknown current coefficients. The scattered fields can then be calculated by summing the radiated fields from each mode on the patch at the given scattering angle.

Results

Computer programs have been written to evaluate the elements of the impedance and resistance matrices and then solve matrix equation (25). As mentioned previously, only the first row of each Z^{pqmn} matrix is calculated by numerical integration. The rest of each submatrix is then filled in by rearranging the elements of the first row. Also, because the Z_{xy}^{pqmn} and Z_{yx}^{pqmn} submatrices are related, only the Z_{xy}^{pqmn} submatrix is evaluated by numerical integration. If results are needed over a band of frequencies, it is only necessary to compute the impedance matrix at a few widely spaced frequencies. The impedance matrix for other frequencies can be found by interpolating each element of the impedance matrices. The number of frequency points at which the impedance matrix must be calculated by numerical integration depends on the span of frequency to be covered. This approach has been used with entire domain basis functions (ref. 12). As mentioned previously, the terms of the resistance matrix do not depend on frequency and need to be calculated only once. The excitation vector, however, does depend on frequency and must be calculated for each frequency. After all the terms were evaluated for a given frequency, the system of equations was solved on the computer by using an IMSL library routine that solves a general complex system of equations and performs iterative improvement on the solution vector.

When modeling the current distribution on the patch, it is necessary to chose M and N large enough to sufficiently approximate the true current distribution. Previous results (ref. 1) have shown that $M = N = 7$ is sufficiently large enough to model the current on the patch when the patch size is close to the size required for the first resonance. Extensive calculations have shown that for the swept frequency results presented, $M = N = 12$ is sufficient for modeling the patch current in the frequency band chosen. In figure 2 the calculated scattering from a rectangular microstrip patch is shown as a function of frequency, where the scattering is measured in dBsm (dB/m^2). As indicated in the figure, there is no significant difference between $M = N = 12$ and $M = N = 16$. However, a slight difference is noted in the scattering response, depending on the number of frequencies at which the impedance matrix was calculated by numerical integration. For the $F = 3$ responses shown, the impedance matrix was calculated at frequencies of 6.0 GHz, 10.0 GHz, and 12.0 GHz. At frequencies between these three points, the impedance matrix was found by quadratic interpolation. The $F = 5$ responses were calculated essentially the same way with the addition of two more frequency points, 8.0 GHz and 12.0 GHz, where the impedance matrix was calculated by numerical integration. The addition of more points, i.e., $F > 5$, made no noticeable difference in the scattering

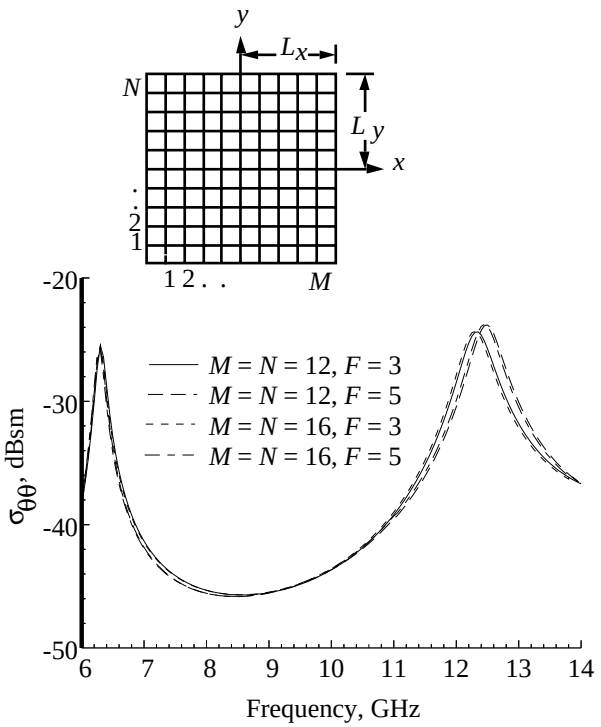

Figure 2. Calculated scattering from a perfectly conducting rectangular microstrip patch antenna. $L_x = 0.75$ cm; $L_y = 0.75$ cm; $d = 0.07874$ cm; $\epsilon_r = 2.33$; Loss tangent = 0.001; $(\theta^i, \phi^i) = (60°, 180°)$.

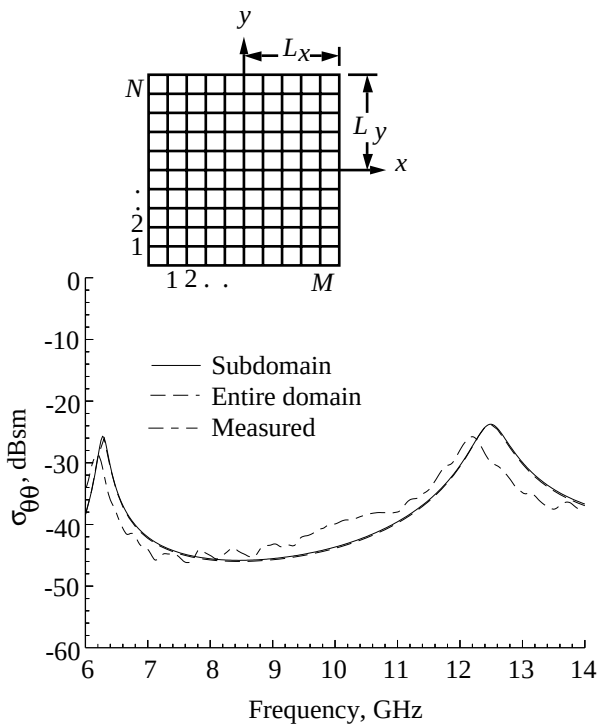

Figure 3. Calculated and measured scattering from a perfectly conducting rectangular microstrip patch antenna. $L_x = 0.75$ cm; $L_y = 0.75$ cm; $d = 0.07874$ cm; $\epsilon_r = 2.33$; Loss tangent = 0.001; $(\theta^i, \phi^i) = (60°, 180°)$.

response. All the following calculated results have been performed with $M = N = 12$ and $F = 5$.

Initially, the radar cross section of four microstrip patches, each with a constant resistance profile, was measured. The computed and measured responses for a perfectly conducting patch are shown in figure 3. The subdomain result was calculated as described above and agrees extremely well with the entire domain result calculated by J. T. Aberle (Arizona State University, private communication). The result measured in the Experimental Test Range (ETR) at the NASA Langley Research Center is slightly shifted in frequency and slightly lower than expected. This is not totally unexpected and can be attributed to the physical tolerances of the patch shape, dielectric constant, and dielectric thickness. The rapid fluctuations seen in the measured data are most likely due to imperfections in the background subtraction performed when processing the radar range data. These subtractions are necessary to approximate the response of the patch on an infinitely large grounded dielectric slab. Although the measured and calculated data do not exhibit as close agreement as is evident in the subdomain and entire domain data, the relative position of the resonant peaks and the scattering levels are fairly close.

The components of the scattered field for other polarizations are shown in figure 4. The $\sigma_{\phi\phi}$ response shows a resonant peak at the same frequency as the $\sigma_{\theta\theta}$ response but also contains a peak in the center of the band where the $\sigma_{\theta\theta}$ response does not. The upper resonant peak in the $\sigma_{\theta\theta}$ response is not evident in the $\sigma_{\phi\phi}$ response. The cross-polarized components, $\sigma_{\theta\phi}$ and $\sigma_{\phi\theta}$, are both the same and show all the peaks of the previous two responses. The current density on the patch when illuminated with a $\widehat{\theta}$-polarized plane wave as in figure 3, is shown in figure 5. The $\widehat{x}$ and $\widehat{y}$ components of the current are shown at the first and second resonances of the patch. At the first resonance the current resembles the expected sinusoidal distribution. At the second resonance this is also the case, although a whole period of the sinusoid is now evident.

Calculations similar to those described above have been performed for a patch with a surface resistance of 5 Ω over the entire patch. The calculated and measured results for $\sigma_{\theta\theta}$ are shown in figure 6. Agreement in this case, is not as good as in the previous

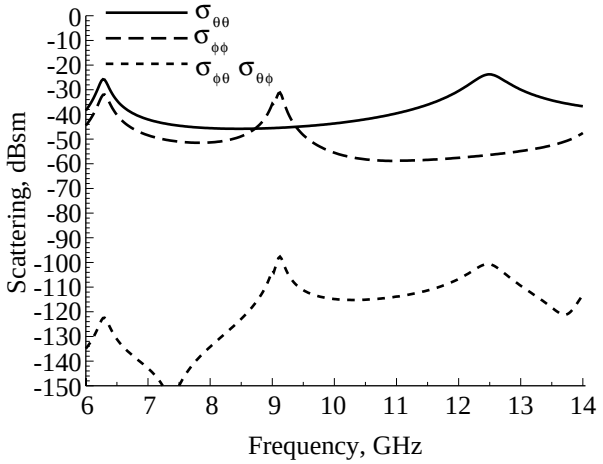

Figure 4. Scattering from a perfectly conducting rectangular microstrip patch as a function of frequency and polarization. $L_x = 0.75$ cm; $L_y = 0.75$ cm; $d = 0.07874$ cm; $\epsilon_r = 2.33$; Loss tangent = 0.001; $(\theta^i, \phi^i) = (60°, 180°)$.

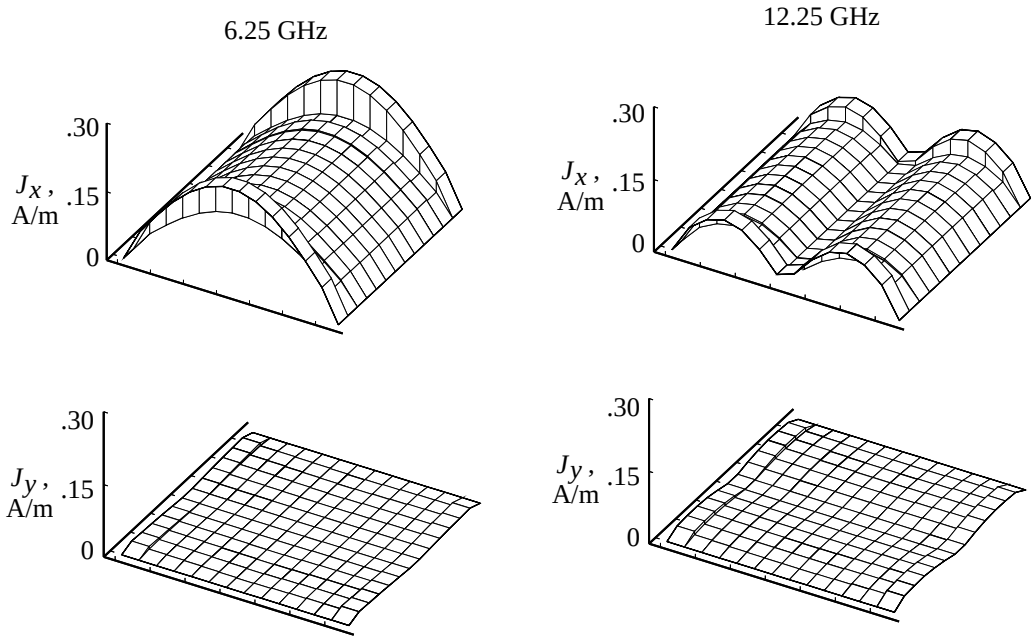

Figure 5. Surface current density J at the first and second resonances on the perfectly conducting patch described in figure 3.

case, but the general shape of the measured data is evident. Note that the peaks in the response have decreased and broadened compared with the perfectly conducting patch. The complete set of scattering results are shown in figure 7. The decrease and broadening of the peaks is seen in each of the responses. The surface resistance was then increased to 11 Ω over the entire patch. The measured and calculated results for $\sigma_{\theta\theta}$ are shown in figure 8. The agreement between the two in this case is quite good across most of the frequency range with some disagreement noted from 7.0–9.0 GHz. As expected, the resonant peaks in the response have decreased and broadened in shape. The current distribution on the patch is shown in figure 9. Although the general shape of the current distribution is the same as for the perfectly conducting patch, the amplitude has been considerably reduced. The $\sigma_{\theta\theta}$ response for a patch with a constant surface resistivity of 20 Ω is shown in figure 10. The calculated and measured results for this case agree across most of the frequency band with only minor discrepancies at the lower frequencies. This is thought to have been caused by the measurement process, as evidenced by the rapid fluctuations in the measured data at the lower frequencies. With a 20 Ω surface resistance on the patch, the

resonant peaks seen in the previous results are not evident. The radar cross section maintains a monotonic increase as frequency increases. The calculated results for $\sigma_{\theta\theta}$ for these four cases are summarized in figure 11. As mentioned previously, as the surface resistance increases the sharp resonant peaks in the response gradually decrease and spread out. A patch with a surface resistance of 20 Ω has no noticeable peaks in the scattering response. These results suggest that the addition of surface resistance to the patch can be used to reduce the scattering from the patch and could possibly be used to increase the operating bandwidth of the antenna. However, this increase in bandwidth may be at the expense of lowering the gain of the antenna.

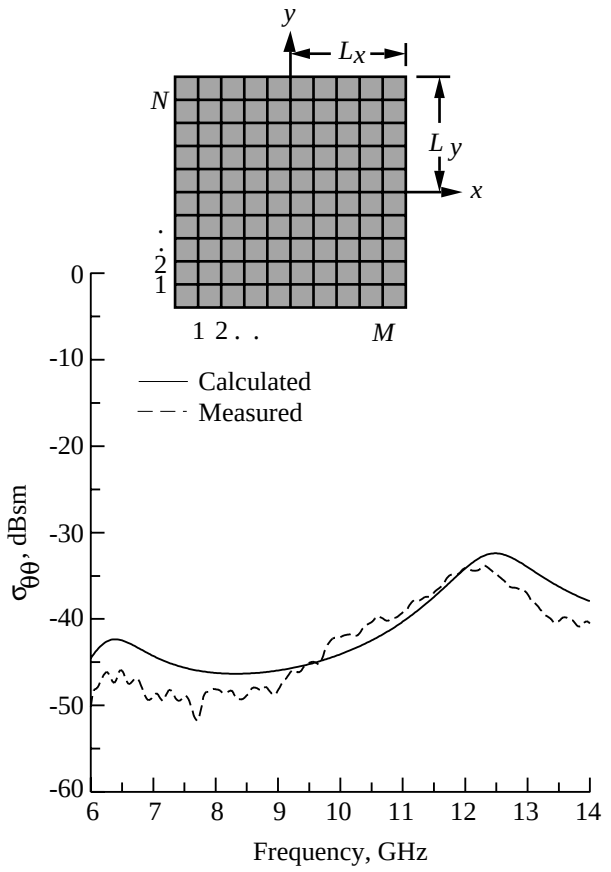

Figure 6. Calculated and measured scattering from a rectangular microstrip patch antenna with constant surface resistance of 5 Ω. $L_x = 0.75$ cm; $L_y = 0.75$ cm; $d = 0.07874$ cm; $\epsilon_r = 2.33$; Loss tangent = 0.001; $(\theta^i, \phi^i) = (60°, 180°)$.

Additional calculations have been performed on patches with surface resistance that varies as a function of position on the patch surface. A patch that is perfectly conducting but has a surface resistance of 5 Ω in each of the corners is shown in figure 12 along with the measured and calculated results for $\sigma_{\theta\theta}$.

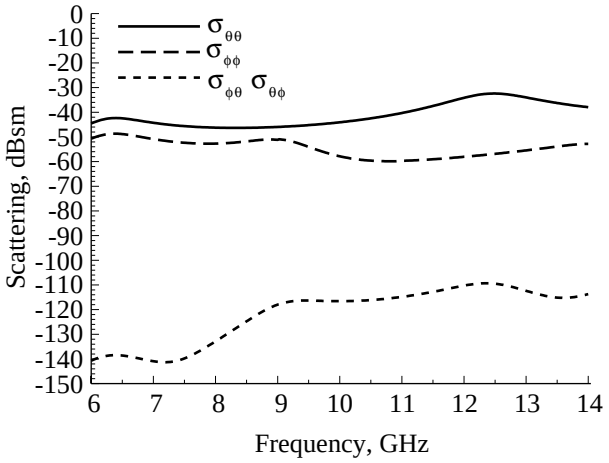

Figure 7. Scattering from a rectangular microstrip patch with a constant surface resistance of 5 Ω as a function of frequency and polarization. $L_x = 0.75$ cm; $L_y = 0.75$ cm; $d = 0.07874$ cm; $\epsilon_r = 2.33$; Loss tangent = 0.001; $(\theta^i, \phi^i) = (60°, 180°)$.

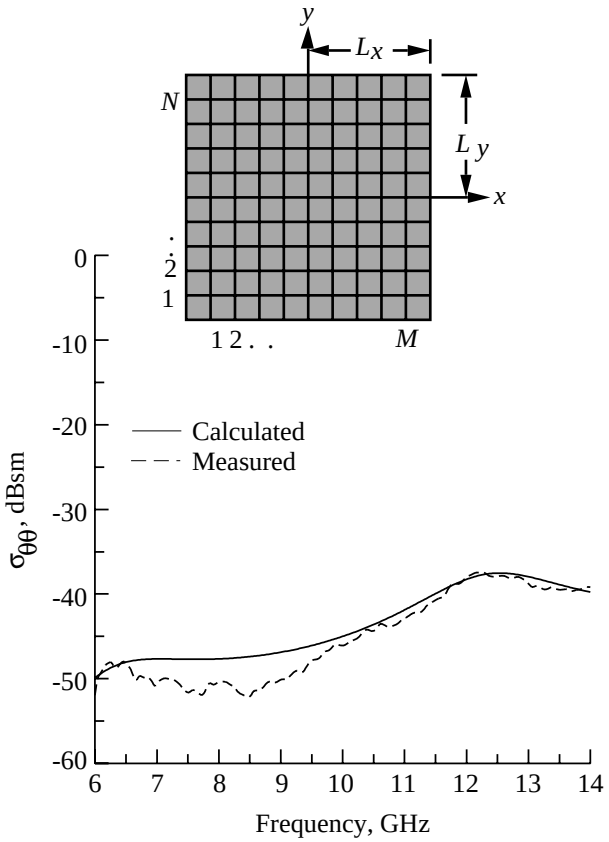

Figure 8. Calculated and measured scattering from a rectangular microstrip patch antenna with constant surface resistance of 11 Ω. $L_x = 0.75$ cm; $L_y = 0.75$ cm; $d = 0.07874$ cm; $\epsilon_r = 2.33$; Loss tangent = 0.001; $(\theta^i, \phi^i) = (60°, 180°)$.

Close agreement between the two is seen across the entire frequency band, although the peaks in the

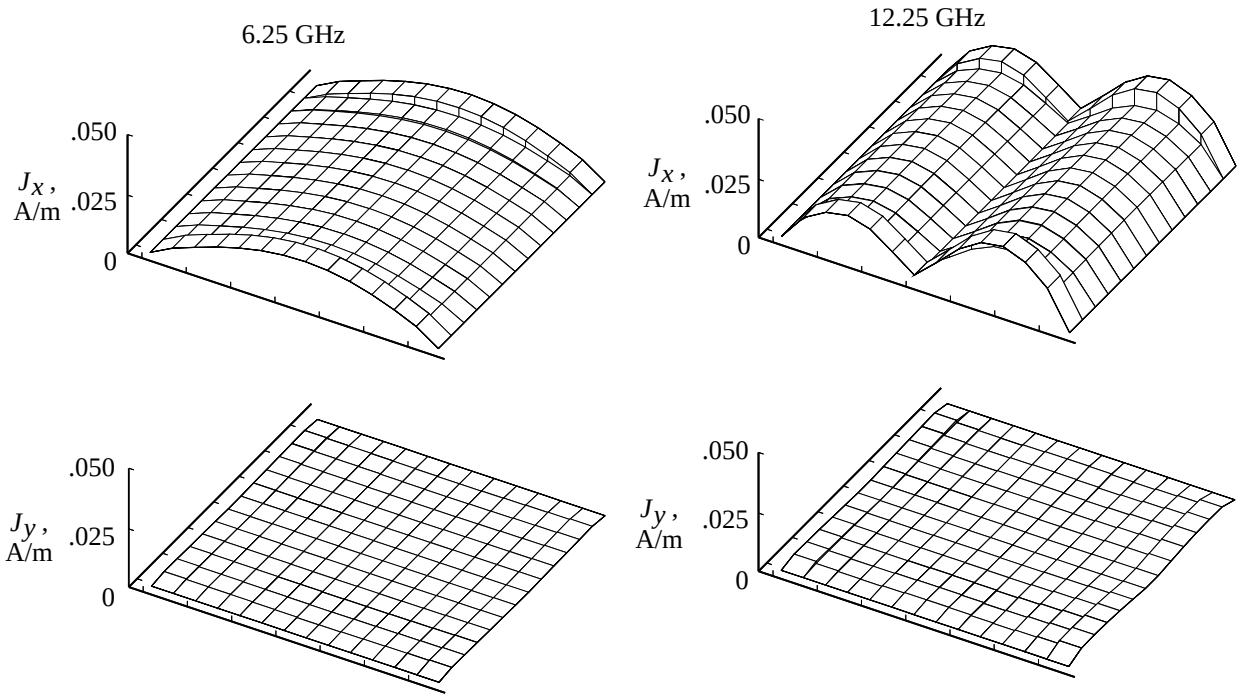

Figure 9. Surface current density J at the first and second resonances on the resistive patch described in figure 8.

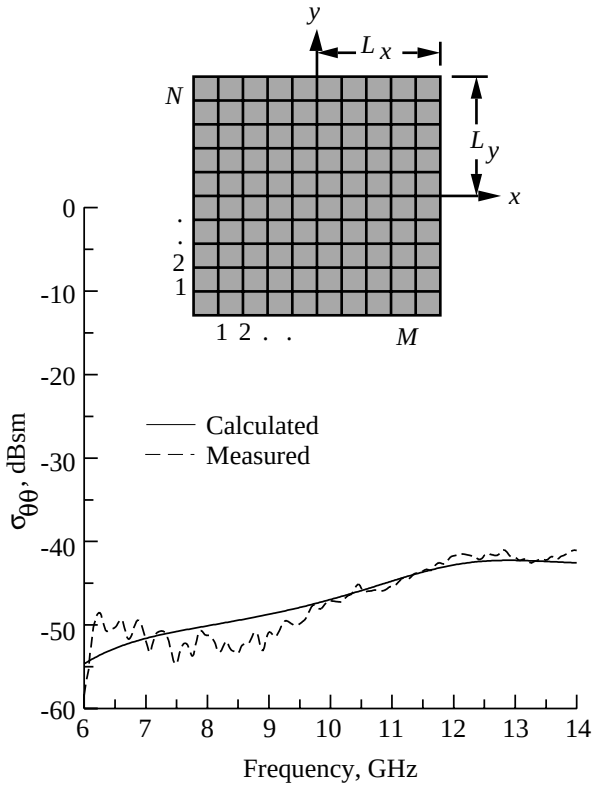

Figure 10. Calculated and measured scattering from a rectangular microstrip patch antenna with constant surface resistance of 20 Ω. $L_x = 0.75$ cm; $L_y = 0.75$ cm; $d = 0.07874$ cm; $\epsilon_r = 2.33$; Loss tangent $= 0.001$; $(\theta^i, \phi^i) = (60°, 180°)$.

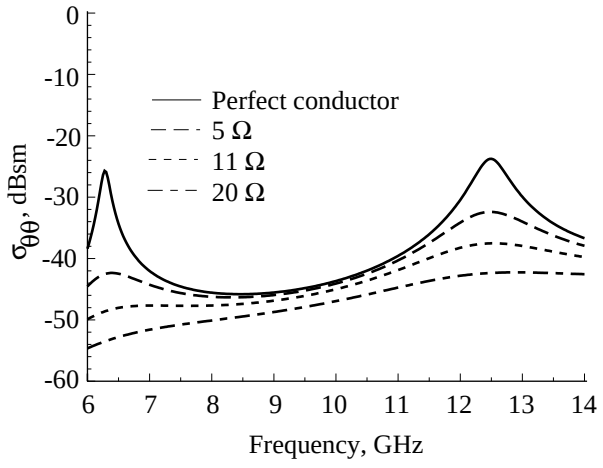

Figure 11. Scattering from a rectangular microstrip patch antenna as a function of frequency and surface resistance. $L_x = 0.75$ cm; $L_y = 0.75$ cm; $d = 0.07874$ cm; $\epsilon_r = 2.33$; Loss tangent $= 0.001$; $(\theta^i, \phi^i) = (60°, 180°)$.

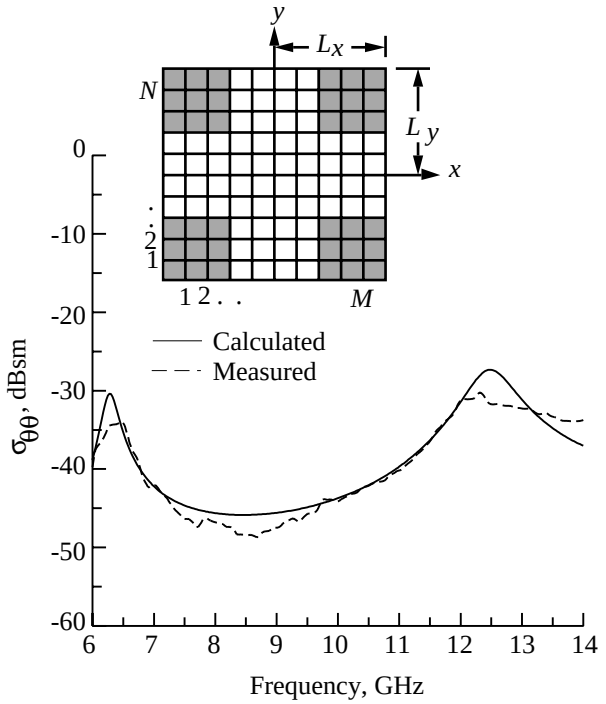

Figure 12. Calculated and measured scattering from a rectangular microstrip patch antenna with surface resistance of $R_s = 5\ \Omega$ for $0.375\ \text{cm} < (|x| \text{ and } |y|) < 0.75\ \text{cm}$. $L_x = 0.75$ cm; $L_y = 0.75$ cm; $d = 0.07874$ cm; $\epsilon_r = 2.33$; Loss tangent $= 0.001$; $(\theta^i, \phi^i) = (60°, 180°)$.

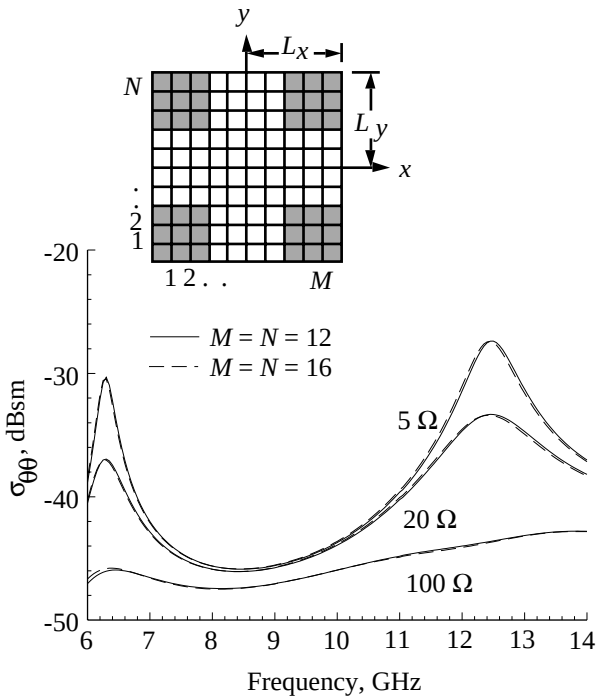

Figure 13. Calculated results of scattering from a rectangular microstrip patch antenna with surface resistance R_s for $0.375\ \text{cm} < (|x| \text{ and } |y|) < 0.75\ \text{cm}$. $L_x = 0.75$ cm; $L_y = 0.75$ cm; $d = 0.07874$ cm; $\epsilon_r = 2.33$; Loss tangent $= 0.001$; $(\theta^i, \phi^i) = (60°, 180°)$.

measured response are not as high as was predicted. This discrepancy may have been caused by imperfections in the shape of the patch. In order to ensure that enough subdomains were used to model the current for this patch, additional calculations were performed with a higher number of subdomains, $M = N = 16$, and higher resistance on the patch corners. These results are shown in figure 13 along with results for $M = N = 12$. As the resistance on the corners of the patch is increased, discontinuities in the current density may result. To accurately model this, a larger number of subdomains may be necessary. However, little difference in the results is seen in the figure with resistance in the corners as high as 100 Ω. The current distributions on the patch described in figure 12 at the two resonant peaks are shown in figure 14 and are similar to those shown previously for patches with a constant surface resistance. A similar patch and the accompanying $\sigma_{\theta\theta}$ results are shown in figure 15. In this case the patch is perfectly conducting in the center and has a 5 Ω surface resistance around the perimeter. The resonant peaks in the response are lower than those of the previous response, as is expected with the addition of resistive material on a greater portion of the patch. A microstrip patch with a 5 Ω surface resistivity on the patch edges is shown in figure 16. The resistance in this case is on the patch edges that have the higher current density for the given excitation. A similar patch is shown in figure 17, but in this case the 5 Ω surface resistance is on the patch edges that have the lower current density for the given excitation. It is interesting to note that the first resonance in figure 16 is considerably lower than the first resonance in figure 17, although the levels at the second resonance for each case are nearly the same. A similar patch is shown in figure 18, but the surface resistance on one of the patch edges has been increased to 20 Ω. The predicted shape of the response can be seen in the measured data, although a frequency shift is clearly evident. As expected, with the increase in the surface resistance on the patch the level of the scattered field decreases. As a final example, a patch that has a 5 Ω surface resistance above the diagonal and is perfectly conducting below the diagonal has been analyzed. This is shown in figure 19 along with the calculated and measured radar cross section $\sigma_{\theta\theta}$. The data show close agreement on the lower portion of

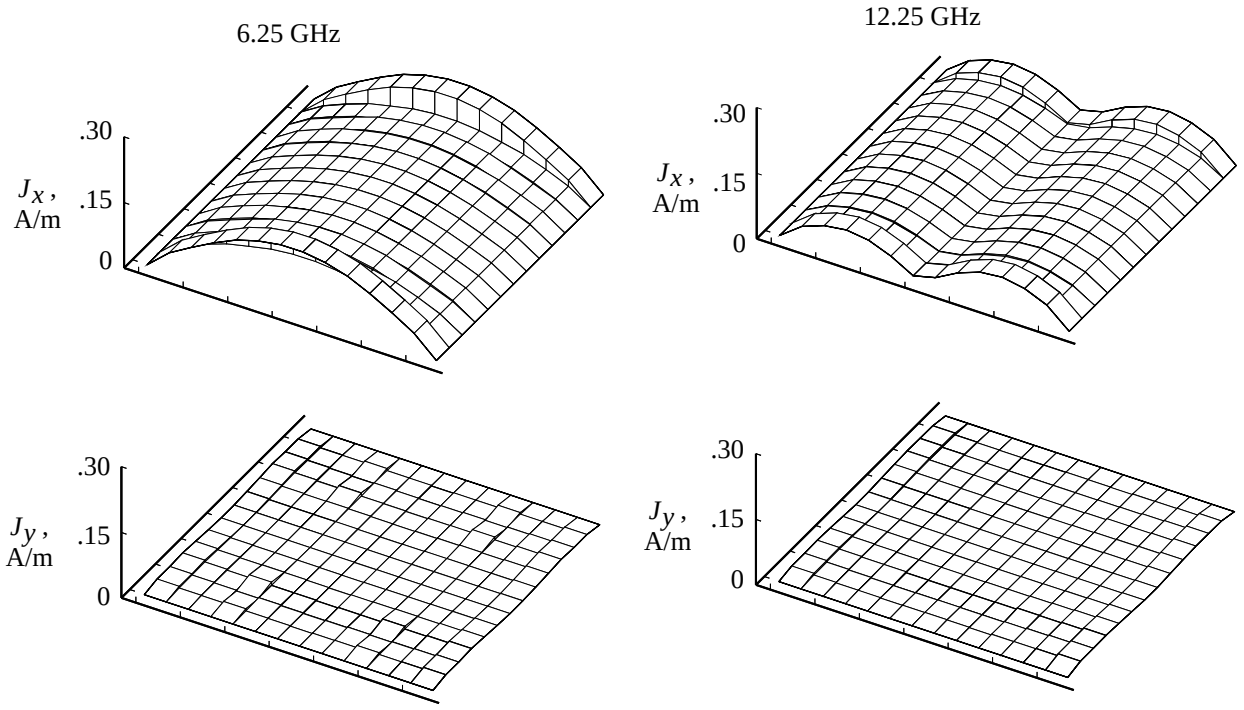

Figure 14. Surface current density J at the first and second resonances on the patch described in figure 12.

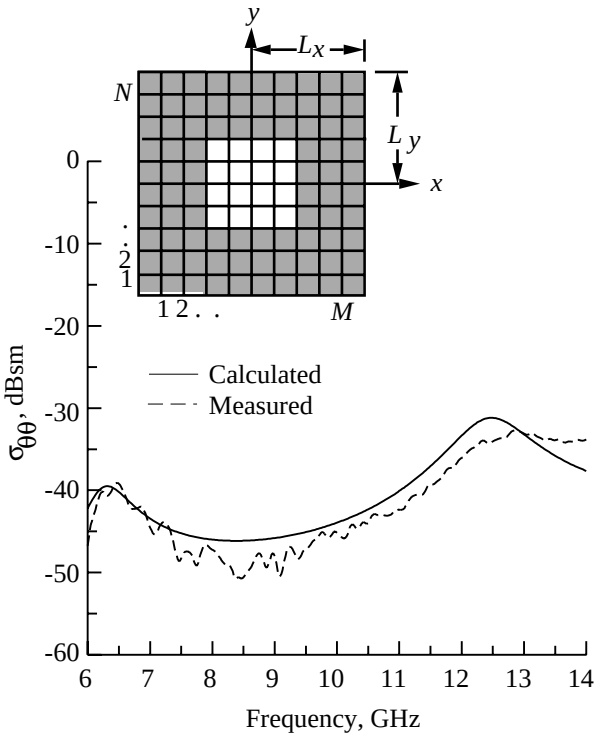

Figure 15. Calculated and measured scattering from a rectangular microstrip patch antenna with surface resistance of $R_s = 5\ \Omega$ for 0.375 cm $< (|x|$ or $|y|) <$ 0.75 cm. $L_x = 0.75$ cm; $L_y = 0.75$ cm; $d = 0.07874$ cm; $\epsilon_r = 2.33$; Loss tangent $= 0.001$; $(\theta^i, \phi^i) = (60°, 180°)$.

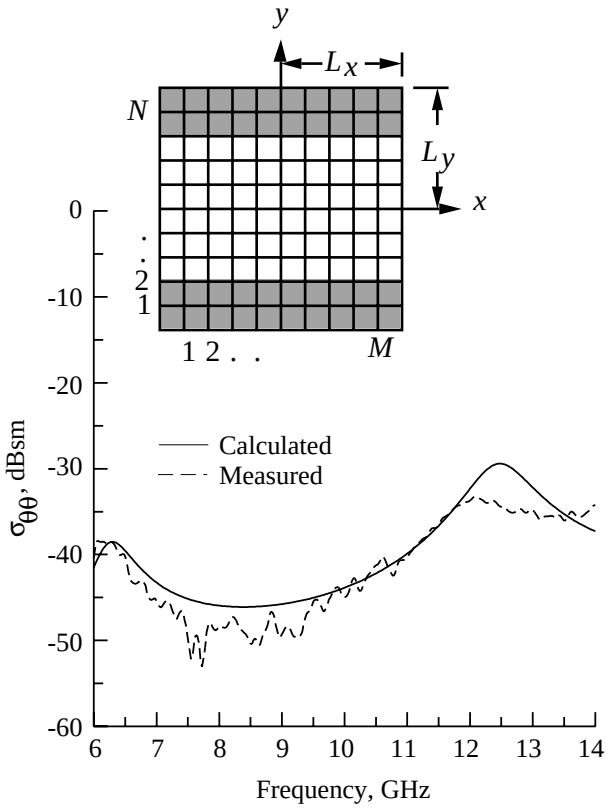

Figure 16. Calculated and measured scattering from a rectangular microstrip patch antenna with surface resistance of $R_s = 5\ \Omega$ for 0.375 cm $< |y| <$ 0.75 cm. $L_x = 0.75$ cm; $L_y = 0.75$ cm; $d = 0.07874$ cm; $\epsilon_r = 2.33$; Loss tangent $= 0.001$; $(\theta^i, \phi^i) = (60°, 180°)$.

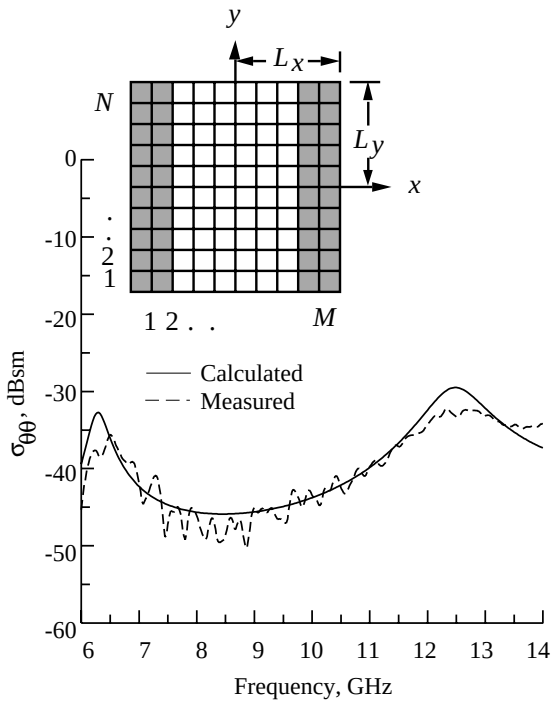

Figure 17. Calculated and measured scattering from a rectangular microstrip patch antenna with surface resistance of $R_s = 5\ \Omega$ for $0.375\ \text{cm} < |x| < 0.75\ \text{cm}$. $L_x = 0.75$ cm; $L_y = 0.75$ cm; $d = 0.07874$ cm; $\epsilon_r = 2.33$; Loss tangent $= 0.001$; $(\theta^i, \phi^i) = (60°, 180°)$.

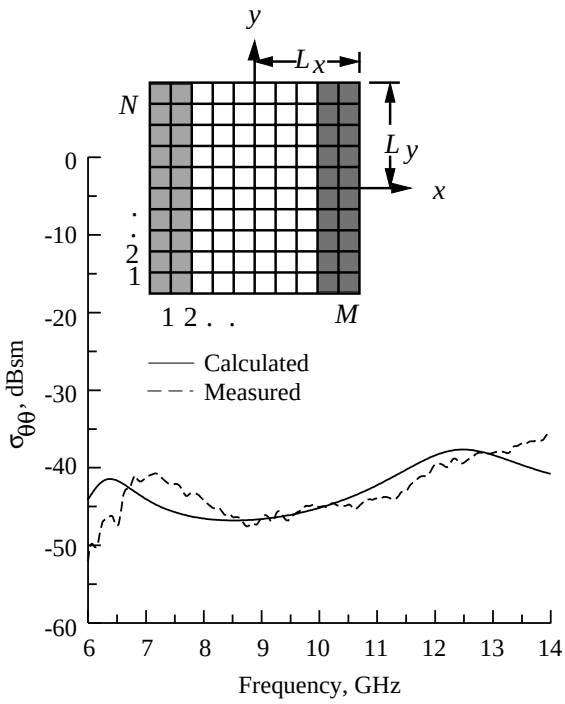

Figure 18. Calculated and measured scattering from a rectangular microstrip patch antenna with surface resistance of $R_s = 5\ \Omega$ for $-0.75\ \text{cm} < x < -0.375\ \text{cm}$ and $R_s = 20\ \Omega$ for $0.375\ \text{cm} < x < 0.75\ \text{cm}$. $L_x = 0.75$ cm; $L_y = 0.75$ cm; $d = 0.07874$ cm; $\epsilon_r = 2.33$; Loss tangent $= 0.001$; $(\theta^i, \phi^i) = (60°, 180°)$.

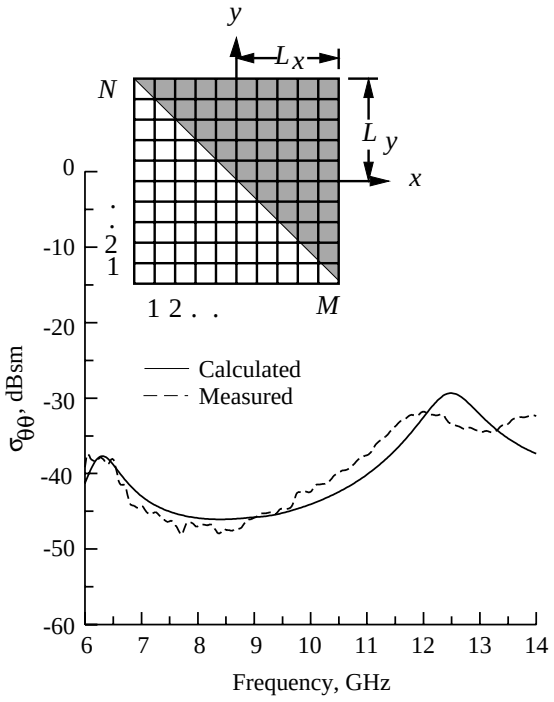

Figure 19. Calculated and measured scattering from a rectangular microstrip patch antenna with surface resistance of $R_s = 5\ \Omega$ above the patch diagonal. $L_x = 0.75$ cm; $L_y = 0.75$ cm; $d = 0.07874$ cm; $\epsilon_r = 2.33$; Loss tangent $= 0.001$; $(\theta^i, \phi^i) = (60°, 180°)$.

the frequency band but have some differences on the upper portion of the frequency band. As before, this was thought to have been caused by imperfections of the patch shape.

Conclusions

This paper has described scattering from rectangular microstrip patches with a surface resistance R_s that is allowed to vary as a function of position on the patch surface. The boundary condition for the electric field was used to derive an integral equation for the electric current that resides on the patch surface. Piecewise linear subdomain basis functions were used to model the current distribution on the patch surface. The necessary terms for representing the surface resistance on the patch were derived and were included in the equation in the form of a resistance matrix. The system of equations was then solved with standard solution techniques available on the computer.

A variety of test cases were performed to ensure the validity of the theory and the accuracy of the computer codes. First, test cases were run for patches with a constant surface resistance. Additional cases were then run for patches with a surface resistance that varied as a function of position on the patch surface. Scattering results, $\sigma_{\theta\theta}$, measured in the Experimental Test Range at the Langley Research Center were compared with the predicted values. In all cases satisfactory agreement between the measured data and the calculated data was noted. However, slight differences were seen in some cases and have been attributed to physical imperfections of the patch shapes, the finite size of the ground plane used, and errors in the radar range background subtraction process. Scattering results for other polarizations have also been calculated and presented.

The addition of resistance on the surface of a microstrip patch antenna has been shown to decrease the scattered energy from the antenna. A resistance of 20 Ω on the entire surface of the patch totally removed the sharp resonant peaks evident in the frequency response of the perfectly conducting patch. In addition to reducing the scattering from a microstrip patch antenna, it may also be possible to increase the impedance bandwidth of the antenna with resistance on the antenna surface if the decrease in the antenna gain can be tolerated.

NASA Langley Research Center
Hampton, VA 23681-0001
May 24, 1993

References

1. Bailey, M. C.; and Deshpande, M. D.: Integral Equation Formulation of Microstrip Antennas. *IEEE Trans. Antennas & Propag.*, vol. AP-30, no. 4, July 1982, pp. 651–656.
2. Deshpande, M. D.; and Bailey, M. C.: Input Impedance of Microstrip Antennas. *IEEE Trans. Antennas & Propag.*, vol. AP-30, no. 4, July 1982, pp. 645–650.
3. Bailey, M. C.; and Deshpande, M. D.: *Analysis of Rectangular Microstrip Antennas.* NASA TP-2276, 1984.
4. Pozar, David M.: Input Impedance and Mutual Coupling of Rectangular Microstrip Antennas. *IEEE Trans. Antennas & Propag.*, vol. AP-30, no. 6, Nov. 1982, pp. 1191–1196.
5. Pozar, David M.; and Schaubert, Daniel H.: Analysis of an Infinite Array of Rectangular Microstrip Patches With Idealized Probe Feeds. *IEEE Trans. Antennas & Propag.*, vol. AP-32, no. 10, Oct. 1984, pp. 1101–1107.
6. Aberle, J. T.; and Pozar, D. M.: Radiation and Scattering From Circular Microstrip Patches. *Antennas and Propagation—1989 IEEE APS International Symposium, Volume I*, IEEE Catalog No. CH2654-2/89, IEEE Antennas and Propagation Soc., 1989, pp. 438–441.
7. Aberle, James T.; and Pozar, David M.: Analysis of Infinite Arrays of One- and Two-Probe-Fed Circular Patches. *IEEE Trans. Antennas & Propag.*, vol. 38, no. 4, Apr. 1990, pp. 421–432.
8. Aberle, J. T.; and Pozar, D. M.: Analysis of Infinite Arrays of Probe-Fed Rectangular Microstrip Patches Using a Rigorous Feed Model. *IEE Proc.*, pt. H, vol. 136, no. 2, Apr. 1989, pp. 110–119.
9. Aberle, James T.; and Pozar, David M.: Accurate and Versatile Solutions for Probe-Fed Microstrip Patch Antennas and Arrays. *Electromagnetics*, vol. 11, no. 1, Jan.–Mar. 1991, pp. 1–19.
10. Pozar, David M.: Radiation and Scattering From a Microstrip Patch on a Uniaxial Substrate. *IEEE Trans. Antennas & Propag.*, vol. AP-35, no. 6, June 1987, pp. 613–621.
11. Aberle, James T.; Pozar, David M.; and Birtcher, Craig R.: Evaluation of Input Impedance and Radar Cross Section of Probe-Fed Microstrip Patch Elements Using an Accurate Feed Model. *IEEE Trans. Antennas & Propag.*, vol. 39, no. 12, Dec. 1991, pp. 1691–1696.
12. Newman, Edward H.; and Forrai, David: Scattering From a Microstrip Patch. *IEEE Trans. Antennas & Propag.*, vol. AP-35, no. 3, Mar. 1987, pp. 245–251.
13. Jackson, David R.: The RCS of a Rectangular Microstrip Patch in a Substrate-Superstrate Geometry. *IEEE Trans. Antennas & Propag.*, vol. 38, no. 1, Jan. 1990, pp. 2–8.
14. Bailey, M. C.; and Deshpande, M. D.: Analysis of Elliptical and Circular Microstrip Antennas Using Moment Method. *IEEE Trans. Antennas & Propag.*, vol. 33, no. 9, Sept. 1985, pp. 954–959.
15. Hansen, V.; and Janhsen, A.: Spectral Domain Analysis of Microstrip Arrays Including the Feed Network

With Space-Varying Surface Impedances and Lumped Elements. *Electromagnetics*, vol. 11, no. 1, Jan.–Mar. 1991, pp. 69–88.

16. Hall, Richard C.; and Mosig, Juan R.: The Analysis of Coaxially Fed Microstrip Antennas With Electrically Thick Substrates. *Electromagnetics*, vol. 9, 1989, pp. 367–384.

17. Hall, R. C.; and Mosig, J. R.: The Calculation of Mutual Coupling Between Microstrip Antennas With Thick Substrates. *1989 International Symposium Digest—Antennas and Propagation, Volume I*, IEEE Catalog No. CH2654-2/89, IEEE Antennas and Propagation Soc., 1989, pp. 442–445.

18. Mosig, Juan R.: Arbitrarily Shaped Microstrip Structures and Their Analysis With a Mixed Potential Integral Equation. *IEEE Trans. Microw. Theory & Tech.*, vol. 36, no. 2, Feb. 1988, pp. 314–323.

19. Mosig, J. R.; and Gardiol, F. E.: General Integral Equation Formulation for Microstrip Antennas and Scatterers. *IEE Proc.*, pt. H, vol. 132, no. 7, Dec. 1985, pp. 424–432.

20. Senior, T. B. A.: Scattering by Resistive Strips. *Radio Sci.*, vol. 14, no. 5, Sept.–Oct. 1979, pp. 911–924.

21. Senior, T. B. A.: Backscattering From Resistive Strips. *IEEE Trans. Antennas & Propag.*, vol. AP-27, no. 6, Nov. 1979, pp. 808–813.

22. Senior, Thomas B. A.: Approximate Boundary Conditions. *IEEE Trans. Antennas & Propag.*, vol. AP-29, no. 5, Sept. 1981, pp. 826–829.

23. Senior, Thomas B. A.: Combined Resistive and Conductive Sheets. *IEEE Trans. Antennas & Propag.*, vol. AP-33, no. 5, May 1985, pp. 577–579.

24. Senior, T. B. A.; and Liepa, V. V.: Backscattering From Tapered Resistive Strips. *IEEE Trans. Antennas & Propag.*, vol. AP-32, no. 7, July 1984, pp. 747–751.

25. Hall, R. C.; and Mittra, R.: Scattering From a Periodic Array of Resistive Strips. *IEEE Trans. Antennas & Propag.*, vol. AP-33, no. 9, Sept. 1985, pp. 1009–1011.

26. Haupt, Randy L.; and Liepa, Valdis V.: Synthesis of Tapered Resistive Strips. *IEEE Trans. Antennas & Propag.*, vol. AP-35, no. 11, Nov. 1987, pp. 1217–1225.

27. Haupt, Randy L.; and Liepa, Valdis V.: Resistive Tapers That Place Nulls in the Scattering Patterns of Strips. *IEEE Trans. Antennas & Propag.*, vol. 38, no. 7, July 1990, pp. 1117–1119.

28. Rubin, B. J.; and Bertoni, H. L.: Reflection From a Periodically Perforated Plane Using a Subsectional Current Approximation. *IEEE Trans. Antennas & Propag.*, vol. AP-31, no. 6, Nov. 1983, pp. 829–836.

29. Cwik, Thomas A.; and Mittra, Raj: Scattering From a Periodic Array of Free-Standing Arbitrarily Shaped Perfectly Conducting or Resistive Patches. *IEEE Trans. Antennas & Propag.*, vol. AP-35, no. 11, Nov. 1987, pp. 1226–1234.

30. Chang, Albert; and Mittra, Raj: Using Half-Plane Solutions in the Context of MM for Analyzing Large Flat Structures With or Without Resistive Loading. *IEEE Trans. Antennas & Propag.*, vol. AP-38, no. 7, July 1990, pp. 1001–1009.

31. Shalaby, Abdel-Aziz T. K.: Spectral Domain Formulation for Superconducting Microstrip Lines With Arbitrary Strip Thickness. *IEEE Antennas and Propagation Society International Symposium—1992 Digest, Volume Two*, IEEE Catalog No. 92CH3178-1, IEEE Antennas and Propagation Soc., 1992, pp. 990–993.

32. Lyons, W. G.; and Oates, D. E.: Microwave Characterization of High-T_c Superconducting Thin Films and Devices. *IEEE Antennas and Propagation Society International Symposium—1992 Digest, Volume Four*, IEEE Catalog No. 92CH3178-1, IEEE Antennas and Propagation Soc., 1992, p. 2256.

REPORT DOCUMENTATION PAGE

Form Approved
OMB No. 0704-0188

1. AGENCY USE ONLY *(Leave blank)*	2. REPORT DATE	3. REPORT TYPE AND DATES COVERED
	August 1993	Technical Paper

4. TITLE AND SUBTITLE
Analysis of Microstrip Patch Antennas With Nonzero Surface Resistance

5. FUNDING NUMBERS
WU 505-64-20-54

P1L162211AH85

6. AUTHOR(S)
David G. Shively and M. C. Bailey

7. PERFORMING ORGANIZATION NAME(S) AND ADDRESS(ES)
Joint Research Program Office
Electronics Integration Directorate
Communications Electronics Command
Langley Research Center
Hampton, VA 23681-0001

NASA Langley Research Center
Hampton, VA 23681-0001

8. PERFORMING ORGANIZATION REPORT NUMBER
L-17219

9. SPONSORING/MONITORING AGENCY NAME(S) AND ADDRESS(ES)
U.S. Army Communications Electronics Command
Fort Monmouth, NJ 07703-5603
and
National Aeronautics and Space Administration
Washington, DC 20546-0001

10. SPONSORING/MONITORING AGENCY REPORT NUMBER
NASA TP-3362

CECOM TR-93-E-2

11. SUPPLEMENTARY NOTES
Shively: Joint Research Program Office, EID-CECOM, Langley Research Center, Hampton, VA;
Bailey: Langley Research Center, Hampton, VA.

12a. DISTRIBUTION/AVAILABILITY STATEMENT
Unclassified–Unlimited

Subject Category 32

12b. DISTRIBUTION CODE

13. ABSTRACT *(Maximum 200 words)*
The scattering properties of a microstrip patch antenna with nonzero surface impedance are examined. The electric field integral equation for a current element on a grounded dielectric slab is developed for a rectangular geometry by using Galerkin's technique with subdomain piecewise linear basis functions. The integral equation includes a resistive boundary condition on the surface of the patch. The incident field on the patch is expressed as a function of incidence angle. The resulting system of equations is then solved for the unknown current modes on the patch, and the radar cross section is calculated for a given scattering angle. Theoretical results in the form of radar cross section as a function of frequency are compared with results measured at the NASA Langley Research Center.

14. SUBJECT TERMS
Antennas; Scattering; Surface resistance

15. NUMBER OF PAGES
16

16. PRICE CODE
A03

17. SECURITY CLASSIFICATION OF REPORT	18. SECURITY CLASSIFICATION OF THIS PAGE	19. SECURITY CLASSIFICATION OF ABSTRACT	20. LIMITATION OF ABSTRACT
Unclassified	Unclassified		